

Unpaired Depth Super-Resolution in the Wild

Aleksandr Safin¹, Maxim Kan^{1*}, Nikita Drobyshev^{1*}, Oleg Voynov¹,
Alexey Artemov¹, Alexander Filippov², Denis Zorin^{3,1}, Evgeny Burnaev¹

¹ Skolkovo Institute of Science and Technology, ² Huawei Noah’s Ark Lab, ³ New York University

{aleksandr.safin, maxim.kan, nikita.drobyshev, oleg.voinov, a.artemov}@skoltech.ru,

dzorin@cs.nyu.edu, e.burnaev@skoltech.ru

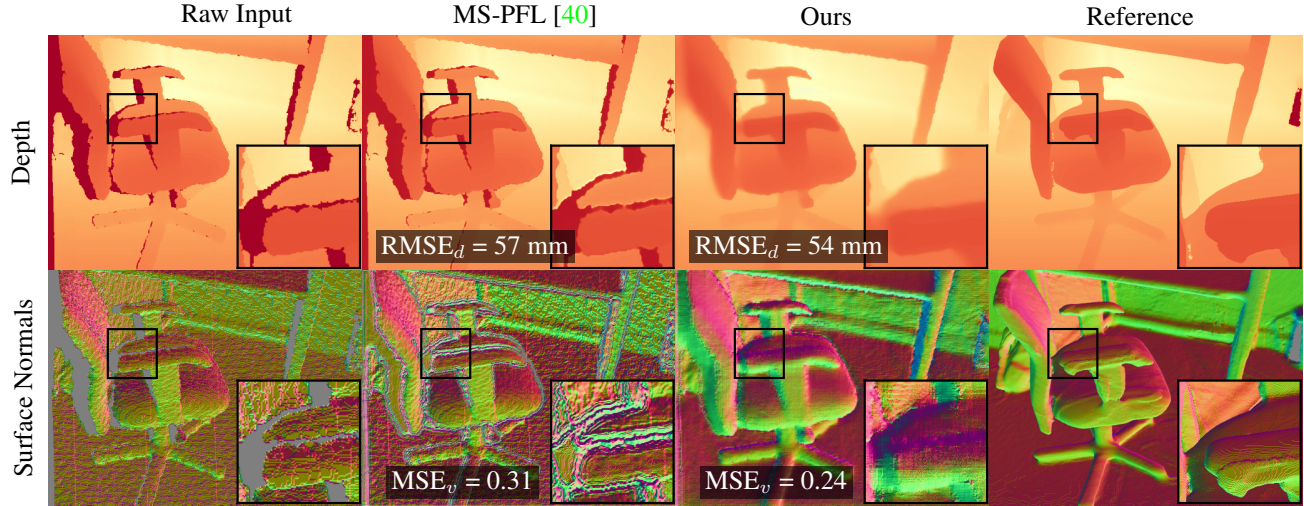


Figure 1: State-of-the-art depth super-resolution methods are designed for clean and complete images, but produce noisy, incomplete results in the wild. In contrast, our novel *unpaired* super-resolution method inpaints holes and produces normals closer (MSE_v [39]) to the reference data. $RMSE_d$ is the depth error averaged over the area of valid (non-hole) pixels.

Abstract

Depth maps captured with commodity sensors are often of low quality and resolution; these maps need to be enhanced to be used in many applications. State-of-the-art data-driven methods of depth map super-resolution rely on registered pairs of low- and high-resolution depth maps of the same scenes. Acquisition of real-world paired data requires specialized setups. Another alternative, generating low-resolution maps from high-resolution maps by subsampling, adding noise and other artificial degradation methods, does not fully capture the characteristics of real-world low-resolution images. As a consequence, supervised learning methods trained on such artificial paired data may not perform well on real-world low-resolution inputs. We consider an approach to depth super-resolution based on learning from unpaired data. While many techniques for unpaired image-to-image translation have been proposed, most fail to deliver effective hole-filling or reconstruct accurate surfaces using depth maps. We propose an unpaired learning method for depth super-resolution, which is based on a learnable degradation model, enhancement component and surface normal estimates as features to produce more accurate depth maps. We propose a benchmark for unpaired depth SR and demonstrate that our method outperforms existing unpaired methods and performs on par with paired.

1. Introduction

Depth images are commonly used in a variety of applications, from 3D scene reconstruction to robotic navigation, user interfaces and photo effects. Depth sensors are becoming standard for everyday devices such as phones and tablets, immensely expanding availability of this type of data and the range of its applications.

However, when acquired with commodity depth cameras, raw depth images come with multiple limitations, most importantly, limited spatial resolution, severe noise levels, and many gaps. Reliably addressing these flaws has been attracting increasing research interest aimed at enhancing the quality of depth images.

Following image super-resolution, where the most success has been made through deep learning [13, 42, 23, 41, 25], convolutional neural networks (CNNs) were applied to depthmap processing [32, 14, 39, 40, 37, 15, 38], where they are commonly trained from paired datasets of low- and high-quality target depth maps. However, acquiring a large real dataset is challenging and requires a customized, calibrated hardware setup; as a result, such methods commonly rely on simple downsampling schemes; this approach is ineffective for training super-resolution models targeting real depth images heavily contaminated by holes and noise.

One way to circumvent this issue is through the use of unpaired learning methods [2, 26, 45], where the model is

*Joint second author contribution.

trained on two datasets, a dataset of inputs and a dataset of targets, with their elements not necessarily forming pairs. While, in principle, one can directly apply existing image-based unpaired methods to depth data, these tend to significantly underperform in practice as they fail to capture the distinctive characteristics of depth images: unlike RGB images, depth images often contain holes, the range of depth values is, in principle, unbounded, and perceptual differences in depths are best captured by depth-specific metrics.

We propose, to the best of our knowledge, the first learning-based method for depth super-resolution for real-world sensor data, using *unpaired* data for training, i.e., a set of raw sensor depth images and a set of high-quality, high-resolution synthetic depth images, without correspondences between images from these sets.

A key aspect of our method is introduction of depth enhancement, that is, a hole-filling and surface denoising method, into the super-resolution pipeline; we demonstrate that coupling depth enhancement and super-resolution tasks results in significantly better results. Our super-resolution pipeline uses a two-part approach to training on unpaired data, inspired by [2]: (1) unpaired learning of degradation, and (2) learning of super-resolution from the degraded depth and self-supervised with real RGB-D images.

Finally it is important to be able to validate the results of depth super-resolution on real sensor depth. However, most of the existing datasets either do not have high-resolution depth corresponding to the low-resolution sensor depth, or have only high-resolution depth. Therefore we created a paired dataset which has both real sensor depth and high-resolution, high-quality depth images. To obtain latter we ray-trace 3D reconstructions of ScanNet [5] indoor scenes, obtained by depth fusion [6] of sensor depth frames. Basing on these, we develop a depth super-resolution and enhancement benchmark, extending a standard evaluation methodology with perceptual measures.

Our evaluation shows that our method outperforms several state-of-the-art image-to-image translation approaches applied to depth in a pure enhancement mode. We likewise outperform straightforward combinations of deep unpaired enhancement (e.g., [8]) and bicubic upsampling, emphasizing the need for a close integration of enhancement and super-resolution parts.

To summarize, our contributions are as follows:

- We introduce the first targeted solution for unpaired depth image super-resolution, that we call *UDSR*. Compared to SOTA unpaired depth enhancement [8] extended to perform SR, we obtain 40% improvement in performance, in terms of a perceptual metric.
- A key component of our method is a new unpaired depth enhancement component that improves unpaired learning by efficiently using RGB image guidance, resulting in better denoising and inpainting for depth im-

ages. We demonstrate our depth enhancement to outperform existing unpaired approaches by 66% in terms of the perceptual MSE_v measure.

- We present a new benchmark for real sensor depth super-resolution and enhancement based on existing datasets [5, 21] and a methodology to compare paired and unpaired approaches.

2. Related Work

Depth super-resolution (SR). Depth super-resolution has been approached from multiple perspectives: filter-based [16, 18], optimization-based [10, 11], and data-driven [32, 14, 22, 39, 40, 37, 13, 42, 23, 41, 25].

In non-learning context, single-frame RGB-guided depth SR has been tackled with joint bilateral filters [18] and filters with adaptive smoothing [16]; optimization-based shape-from-shading approaches [10, 11] relying on photometric constraints and a number of priors. While such techniques are sensor-agnostic, their ability to exploit RGB and depth image priors is limited.

Among data-driven approaches, CNNs have been used in combination with optimization-based methods [32], joint filtering methods [22], as well as with multi-scale image/depth guidance [14, 40]; we use CNNs with explicit RGB guidance but without additional postprocessing. More recently, perceptually-based depth SR [39] enabled more accurate surface reconstruction; we integrate their loss function in our training framework. [37] considered two types of downsampling degradations and introduced a novel depth SR pipeline. Importantly, these methods need aligned pairs of sensor and ground-truth images capturing the same view; differently, in this work we explore an *unpaired learning scenario* where the sets of source and target depth images may depict distinct environments.

Unpaired image SR. Alternative learning-based formulations bypass the need for paired data, greatly simplifying construction of training datasets. Among unpair-image methods, Zero-shot SR [1] relies on self-supervised training from low-resolution images only; other approaches use independent sets of low-resolution and high-resolution images, commonly employing cycle consistency [49] to learn the SR mapping without correspondences between images. Most unpaired systems are trained in multiple stages; Cycle-in-Cycle [45] learns image cleaning during the first cycle and SR in the unpaired setting using the second cycle; Bulat *et al.* [2] learns degradation using an unpaired setup, further performing supervised training for SR; Maeda [26] decomposes SR mapping into a cleaning step trained in an unpaired way and a pseudo-supervised SR network. Our method similarly uses two-stage training.

Depth enhancement [8, 15] encompasses several other subtasks including denoising [46, 19, 20, 9], competition, and inpainting [47, 24, 44, 30, 43]. LapDEN [15] rendered

3D reconstructions in ScanNet [5] to obtain training data for their depth enhancement method; we implement a similar but extended data generation technique and compare our method to this approach.

Unpaired depth enhancement is similar in spirit to unpaired image-to-image translation but requires considerable adaptation of existing image-based methods. Gu *et al.* pioneered a GAN-based unpaired depth enhancement [8] with a four-stage learnable approach, involving hole prediction, image adaptation, degradation, and final enhancement. From a self-supervised perspective, [38] leverages photometric constraints to recover high-quality depth but requires an additional acquisition setup. Learning from unsynchronized low- and high-quality depth frames, [35] proposes a self-supervised approach employing temporal and spatial alignment. Among these methods, we extensively compare to single-image unpaired enhancement [8], combining their approach with non-learnable upsampling.

RGB-D datasets for depth SR. Among RGB-D datasets, Middlebury [34], NYU-Depth V2 [28], SUN RGB-D [36], and the synthetic ICL-NUIM [12] provide RGB-D frames but cannot serve as evaluation data for depth super-resolution since they either do not provide real-world sensor depth or lack corresponding ground truth. Matterport3D [3] is a large-scale dataset with high-quality depth but lacks corresponding depth from less accurate sensors. ToF-Mark [7] contains depth maps from a low-accuracy time-of-flight sensor and a high-accuracy structured light scanner but only provides three frames. Similarly, Redwood [29] consists of RGB-D sequences obtained using a consumer Asus Xtion Live depth camera and point clouds from industrial-grade laser scanner but captures only five scenes.

In the context of depth enhancement, [15] synthesized a paired dataset from ScanNet [5], a large-scale collection of RGB-D scans, using its complete 3D reconstructed models obtained using BundleFusion [6]. These models were ray-casted to obtain image pairs of the same resolution for training neural networks targeting denoising and hole-filling. We extend this approach to our task, additionally creating high-resolution depth images from renderings of 3D reconstructions (Section 4.1). We additionally conduct experiments using synthetic indoor data in InteriorNet [21].

3. Method

3.1. Unpaired Depth Super-Resolution

Task formulation. RGB-D cameras jointly capture pairs (I, D^L) of sensor data, where I is a color image and D^L is a depth map of the scene. In our work L , the source set, contains RGB-D images where the depth map is a low-resolution, noisy image with missing pixel values¹.

¹We assume RGB color images to always come at high resolution.

Learning-based methods use a target set H of reference high-resolution RGB-D images (I, D^H) to learn a mapping from L to H . For sensor and reference images capturing the same scene, a straightforward approach approximates a map $L \rightarrow H$ by a neural network trained from instances $(I, D^L) \in L$ and $(I, D^H) \in H$. However, most commonly, sufficient amount of registered pairs is not available, and source depth images D^L are *synthesized* by downsampling.

In our method, two sets L and H capture different scenes without correspondences between their instances. We seek to estimate the high-resolution, high-quality depth image \hat{D} from the sensor data using the relation $\hat{D} = u_{\text{sr}}(I, D^L)$ where u_{sr} is a mapping between the L and H . An advantage of this approach is that a data-driven mapping is used instead of synthetic downsampling.

Method overview. We represent the SR mapping f_{sr} by a composition $u_{\text{sr}} = u_{\text{enh}} \circ u_{\text{up}}$ of a non-trainable upsampling operation u_{up} (we use bicubic interpolation) and a trainable enhancement mapping u_{enh} . The upsampling operation interpolates the depth image to the resolution of the RGB image; the enhancement mapping inpaints gaps and refines surface normals, improving depth image quality.

Making u_{enh} trainable enables effective use of heterogeneous information such as RGB guidance [14, 39]. To circumvent the lack of paired examples for training u_{enh} , following the recent work on unpaired image SR [26] we construct training *pseudo-examples* by translating H into a set of realistic low-quality depth images, by generating H_{down} , a set of downsampled RGB-D images, followed by using a separate translation network pre-trained in an unpaired way. Thus, we work with depth images of equal spatial resolution but significantly different quality.

Our system consists of two interrelated trainable components, the Translation Component and the Enhancement Component (implementing u_{enh}), trained consecutively using two phases (see Table 1). Compared to the fully unpaired formulation in [26], we use a separate enhancement step similarly to [2], which simplifies training. First, we pre-train the Translation Component using the datasets L and H_{down} in an unpaired manner, obtaining two trained generative networks g_{H2L} and g_{L2H} , implementing coarse mappings $H_{\text{down}} \rightarrow L$ and $L \rightarrow H_{\text{down}}$ (Section 3.2). We freeze the weights of these networks for the subsequent phase.

Then, we use g_{H2L} to synthesize low-quality depth maps D_{degr}^H from samples in H_{down} . Finally, we train the Enhancement Component using the synthesized instances (I, D_{degr}^H) and the real images $(I, D^L) \in L$ (Section 3.3).

For inference (Figure 2), we interpolate the low-resolution depth map D^L to the resolution of the color image using bicubic interpolation. To refine the interpolated depth map into the final high-resolution result \hat{D} , in the Enhancement Component we (1) compute feature maps of

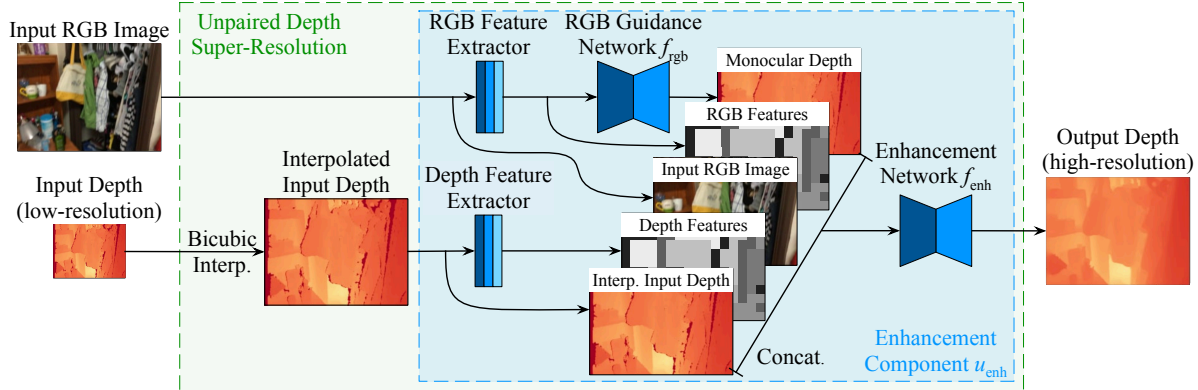


Figure 2: Scheme of depth super-resolution with our Enhancement Component u_{enh} . We first upsample depth via Bicubic interpolation to the target resolution of the color image. Then we employ RGB guidance network f_{rgb} to extract a monocular depth estimate and run feature extractors to obtain photometric and geometric convolutional features. Finally, the enhancement network f_{enh} predicts a refined depth image by fusing this information along with the source RGB-D pair.

Component	Training	Inference
Translation Component	Phase 1: Cycle-consistent unpaired training \rightarrow generate pseudo-examples (Section 3.2)	Not used
Enhancement Component	Phase 2: Supervised training with pseudo-examples (Section 3.3)	Direct prediction

Table 1: Component-wise view of our method.

the input depth and RGB images with convolutional feature extractors, (2) estimate an intermediate depth map with the image guidance network f_{rgb} , and (3) estimate the final depth map from the input images concatenated with their feature maps and the intermediate depth map using the enhancement network f_{enh} .

3.2. Unpaired Training of Translation Component

Unpaired training formulation. We implement an unpaired learning setup for translation between the low-quality set L and the high-quality set H_{down} . Our setup (Figure 3) is somewhat similar to the CycleGAN-based image enhancement formulation [26]: the translation network g_{H2L} learns a desired degradation mapping from the high-quality domain H_{down} to the low-quality domain L , while a concurrent reverse translation network g_{L2H} learns to translate from L to H_{down} . In our case, all depth images in both sets have the same spatial resolution.

Cycle-consistency loss. We use the cycle-consistency loss $\mathcal{L}_{\text{cycle}}$ for high-quality instances in the H_{down} dataset only, for the reconstructed depth $D_{\text{rec}}^H = g_{L2H}(g_{H2L}(D^H))$. The expression for our cycle consistency loss

$$\mathcal{L}_{\text{cycle}} = L_1(D^H, D_{\text{rec}}^H) + \text{MSE}_v(D^H, D_{\text{rec}}^H)$$

includes depth-based L_1 and normals-based MSE_v terms [39] (discussed in Section 3.3).

Depth range loss. As depth values in D^L and D^H have

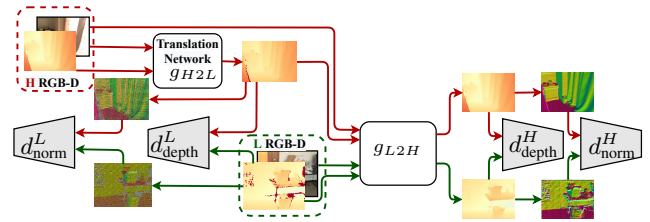


Figure 3: Training scheme for the translation network.

different range and overall distribution, we include

$$\mathcal{L}_{\text{range}} = \lambda_{\text{range}}^L L_1(D_{\text{enh}}^L, D^L) + \lambda_{\text{range}}^H L_1(D_{\text{degr}}^H, D^H)$$

where $D_{\text{enh}}^L = g_{L2H}(D^L)$ and $D_{\text{degr}}^H = g_{H2L}(D^H)$, to prevent both mappings g_{L2H} and g_{H2L} from significantly altering non-zero depth values. The contribution of this loss to the full objective is relatively small, to encourage networks to perform denoising and learn non-identity mappings in non-zero depth regions.

Identity loss. As it is customary with CycleGAN, we penalize changes introduced by the translation network g_{L2H} for targets D^H using the identity objective

$$\mathcal{L}_{\text{idt}} = \lambda_{\text{idt}}^H L_1(g_{L2H}(D^H), D^H).$$

Discriminators and adversarial loss \mathcal{L}_{adv} . We augment the adversarial part with surface normals discriminator networks, ending up with four depth- and normals-based discriminators: d_{depth}^H , d_{norm}^H operating in H_{down} , and d_{depth}^L , d_{norm}^L operating in L . We compute normals using finite differences and use LSGAN [27] formulation for losses.

Similarly to [26], aiming to relax the requirements for the generator and stabilize training, we substitute D^H for D_{rec}^H for discriminator d_{depth}^H operating in the target set.

Full unpaired learning loss. The system is trained by optimizing a loss function discriminating between real and translated images in each respective domain while enforc-

ing cycle-consistency between the translated images:

$$\mathcal{L} = \lambda_{\text{cycle}}^H \mathcal{L}_{\text{cycle}} + \mathcal{L}_{\text{adv}} + \mathcal{L}_{\text{idt}} + \mathcal{L}_{\text{range}}.$$

We select λ_{cycle}^H , λ_{range}^L , λ_{range}^H , λ_{idt}^H to balance contributions of each individual loss term.

3.3. Training the Enhancement Component with Pseudo-Examples

Guidance networks. We pre-train f_{rgb} , a U-Net-like image guidance CNN [33], to estimate the depth map from the color image. We use instances from both datasets L and H_{down} , minimizing L_1 error between D^L and its monocular estimate $f_{\text{rgb}}(I)$ for instances from the set $(I, D^L) \in L$ and an analogous quantity for samples $(I, D^H) \in H_{\text{down}}$. We use a shared decoder but separate encoders for source and target datasets due to a significant difference between their data distributions, and freeze the weights after pre-training.

Enhancement network and full objective. We train the enhancement network f_{enh} together with RGB/depth feature extractors on instances in both datasets. During training, for each input RGB-D image (I, D^L) we compute a monocular depth estimate $f_{\text{rgb}}(I)$, synthesize a degraded instance $D_{\text{degr}}^H = g_{H2L}(D^H)$ on the fly by randomly picking a high-quality depth image D^H , and pass a tuple $(I, D, f_{\text{rgb}}(I))$ to f_{enh} as input. Here D represents either D^L or D_{degr}^H .

For the target dataset H , we treat the high-quality input/output pair (D_{degr}^H, D^H) as a training pseudo-example and minimize the *pseudo-supervised* loss (see details on particular loss functions in sec. 3.4)

$$\begin{aligned} \mathcal{L}^H(f_{\text{enh}}) = & \mathcal{L}_{\text{depth}}(\widehat{D}, D^H; w_{\text{depth}}, \lambda_{\text{depth}}) \\ & + \mathcal{L}_{\text{surf}}(\widehat{D}, D^H; w_{\text{norm}}, \lambda_{\text{surf}}^H) + \lambda_{\text{smooth}}^H \mathcal{L}_{\text{smooth}}(\widehat{N}), \end{aligned}$$

where $\widehat{D} = f_{\text{enh}}(I, D_{\text{degr}}^H)$ and \widehat{N} is its normal image.

For the set L of source images, we aim to preserve the overall content and object boundaries but perform inpainting and denoising. The pair (D^L, D^L) thus acts as a constraint with the goal of regularizing training of the enhancement network. The structure of this *self-supervised* loss is

$$\begin{aligned} \mathcal{L}^L(f_{\text{enh}}) = & \mathcal{L}_{\text{depth}}(\widehat{D}, D^L; w_{\text{depth}}, \lambda_{\text{depth}}^L) \\ & + \lambda_{\text{edge}}^L \mathcal{L}_{\text{edge}}(\widehat{D}, I) + \lambda_{\text{smooth}}^L \mathcal{L}_{\text{smooth}}(\widehat{N}), \end{aligned}$$

where $\widehat{D} = f_{\text{enh}}(I, D^L)$.

The hyperparameters λ_{depth}^L , λ_{edge}^L , $\lambda_{\text{smooth}}^L$, λ_{depth}^H , λ_{surf}^H , $\lambda_{\text{smooth}}^H$ are chosen to level the contribution of each summand, with λ_{depth}^L slightly attenuated to avoid reproducing low-quality inputs. In Appendix we provide values used in our experiments. Our full enhancement objective is

$$\mathcal{L}(f_{\text{enh}}) = \mathcal{L}^H(f_{\text{enh}}) + \mathcal{L}^L(f_{\text{enh}})$$

with $\mathcal{L}^H(f_{\text{enh}})$ providing a useful enhancement target and $\mathcal{L}^L(f_{\text{enh}})$ aiming to maintain performance for real instances.

3.4. Loss Functions

Depth loss. For direct supervision in the source set L and for self-supervision in the target set H we use a combination of pixel-weighted mean absolute error (MAE, L_1) and mean squared error (MSE, L_2), defined by

$$\mathcal{L}_{\text{depth}}(D_1, D_2; w, \lambda_{\text{depth}}) = \sum_{p \in \{1, 2\}} \lambda_{\text{depth}, p} \|w_{\text{depth}, p} \odot (D_1 - D_2)\|_p,$$

where \odot denotes pixel-wise multiplication.

Perceptual surface loss. To enforce accurate surface geometry, we employ perceptual losses [39] defined as weighted p -norms of surface renderings of depth images averaged over three orthogonal light directions e_i :

$$\mathcal{R}_p(D_1, D_2, w_{\text{surf}}) = \frac{1}{3} \sum_{i=1}^3 \|w_{\text{surf}, p} \odot (N_1 - N_2) \cdot e_i\|_p,$$

where N_1 and N_2 are finite-difference estimates of the normal maps from the depth images D_1 and D_2 , respectively. We define $\text{MAE}_v = \mathcal{R}_1$ and $\text{MSE}_v = \mathcal{R}_2$ and set

$$\mathcal{L}_{\text{surf}} = \lambda_{\text{surf}, 1} \text{MAE}_v + \lambda_{\text{surf}, 2} \text{MSE}_v.$$

Boundary loss. To encourage sharp depth discontinuities at object boundaries we adopt the edge-based loss [48]

$$\mathcal{L}_{\text{edge}}(D, I) = |\nabla_h D| e^{-|\nabla_h I|} + |\nabla_v D| e^{-|\nabla_v I|},$$

where ∇_h and ∇_v denote finite differences computed in horizontal and vertical direction.

Denoising loss. To suppress noise and impose spatial smoothness on the normal image N , we minimize total variation [31, 45] expressed by $\mathcal{L}_{\text{smooth}}(N) = \|\nabla_h N\|_2 + \|\nabla_v N\|_2$.

3.5. Evaluation Framework

For direct comparison of unpaired and supervised (paired) methods we propose the following training and evaluation framework. We start from a paired dataset containing low-quality (L) and high-quality RGB-D images (such as H_{down} or H) and adapt it as follows (see Figure 4):



Figure 4: Unpaired methods are trained on disjoint parts A and B, while paired ones have training pairs.

1. We split the dataset into training, validation and test sets, each using a different subset of scenes.
2. We further split the training set into two disjoint parts, also using distinct scenes, Train A and Train B.
3. The unpaired training set U includes low-quality images in Train A and high-quality images in Train B.
4. The supervised training set S combines low-quality images in Train B and high-quality images in Train B.

Method	RMSE \downarrow	RMSE $_h$ \downarrow	RMSE $_d$ \downarrow	MAE \downarrow	MAE $_h$ \downarrow	MAE $_d$ \downarrow	MSE $_v$ \downarrow
LapDEN [15] (sup.)	76.02	165.57	58.40	22.63	92.73	15.92	0.0774
Gu <i>et al.</i> [8]	108.25	193.87	94.32	57.13	120.23	51.73	0.3307
NiceGAN [4]	156.52	410.23	111.45	97.62	324.83	79.45	0.1953
U-GAT-IT [17]	292.80	507.95	261.30	249.54	434.48	235.26	0.1422
CycleGAN [49]	416.57	450.55	407.48	391.21	389.36	392.51	0.1326
UDSR (Ours)	77.07	169.55	63.31	32.99	110.06	27.26	0.1194

Table 2: Enhancement on **ScanNet-RenderScanNet**.

Method	[23] \ddagger	[40] \ddagger	[23] $*$	[40] $*$	[8]+[23]	[8] + B	B + [8]	UDSR
RMSE \downarrow	76.94	75.47	363.51	299.53	<u>107.71</u>	107.96	114.72	86.24
RMSE $_h$ \downarrow	176.41	168.43	1435.45	1163.83	<u>194.11</u>	<u>193.79</u>	323.02	172.60
RMSE $_d$ \downarrow	58.45	60.40	129.03	117.74	94.67	95.02	<u>78.46</u>	74.66
MAE \downarrow	22.16	30.16	109.33	93.70	56.77	57.06	<u>56.30</u>	45.51
MAE $_h$ \downarrow	92.50	113.29	1392.10	1110.62	<u>121.18</u>	121.44	246.53	113.76
MAE $_d$ \downarrow	16.44	23.78	27.11	<u>29.31</u>	51.71	52.01	43.14	40.64
MSE $_v$ \downarrow	0.1637	0.1612	0.2576	<u>0.2485</u>	0.2811	0.2852	0.5202	0.2023

Table 3: SR on **ScanNet-RenderScanNet**. We compare with SRFBN [23], MS-PFL [40] and Gu *et al.* [8]. B denotes Bicubic interpolation was applied. \ddagger and $*$ mark the models trained on (L, H) and (H_{down}, H) pairs respectively.

5. Test set T , obtained at step 1, is the same for both unpaired and supervised methods.

This approach makes it possible to directly compare unsupervised methods trained on U with supervised methods trained on S . Based on this approach, we develop a depth super-resolution and enhancement benchmark, that we describe below.

Method	RMSE $_h$ \downarrow	RMSE $_d$ \downarrow	MAE $_h$ \downarrow	MAE $_d$ \downarrow	MSE $_v$ \downarrow
UDSR *	238.39	203.81	183.73	188.18	0.3934
UDSR ‡	213.28	66.05	135.22	31.01	0.2442
UDSR *	208.58	69.28	135.04	36.27	<u>0.2361</u>
UDSR *	<u>192.00</u>	63.08	<u>119.43</u>	25.44	0.2299
UDSR ‡	376.28	66.53	271.50	29.73	0.4121
UDSR ‡	228.43	71.56	151.09	36.64	0.3512
UDSR $^{\diamond}$	342.05	66.17	279.85	28.83	0.2875
UDSR $^{\diamond}$	177.67	<u>62.75</u>	104.18	<u>24.59</u>	0.4315
UDSR	197.86	60.95	123.50	20.59	0.2605

* Ours with translation network g_{H2L} replaced by CycleGAN [49]

‡ Ours with translation network g_{H2L} trained without surface normal discriminators $d_{\text{norm}}^H, d_{\text{norm}}^L$

* Ours with translation network g_{H2L} trained without MSE $_v$ loss

* Ours with translation network trained without depth range loss

† Ours without f_{rgb}

‡ Ours without any surface normal term loss in Enhancement network

$^{\diamond}$ Ours with enhancement network f_{enh} trained without additional holes

$^{\circ}$ Ours with enhancement network f_{enh} trained without pseudo examples

Table 4: Ablation of SR on **ScanNet-InteriorNet**.

Method	UDSR	B + [8]	[8] + B	[8] + [23]
RMSE \downarrow	81.12	241.20	107.14	107.23
RMSE $_h$ \downarrow	197.86	893.06	<u>297.69</u>	298.18
RMSE $_d$ \downarrow	60.95	109.01	67.85	67.81
MAE \downarrow	27.97	93.51	46.12	45.70
MAE $_h$ \downarrow	123.50	771.49	209.92	209.99
MAE $_d$ \downarrow	20.59	50.50	33.57	33.12
MSE $_v$ \downarrow	0.2605	0.4794	0.3670	0.4250

Table 5: SR on **ScanNet-InteriorNet**.

4. Experiments

4.1. Datasets

Our benchmark includes two training and one testing dataset. Each dataset consists of three sets of RGB-D images: source set L with low-quality, low-resolution depth maps, target set H with high-quality, high-resolution depth maps, and the set H_{down} with the same high-quality depth maps as in the set H but downsampled to the resolution of the set L .

The first training dataset **ScanNet-RenderScanNet** is based on ScanNet [5], which contains RGB-D images captured with Structure depth sensor with 640×480 depth maps and 1280×960 color images. We used these images to build the set L , as we describe below. To get the high-resolution 1280×960 depth maps for the set H_{down} we rendered the 3D models of the ScanNet scenes, reconstructed with Bundle-Fusion [6]. In comparison to the raw depth maps, the depth values in these renderings are defined almost everywhere, and the noise is reduced by depth fusion.

To get high-quality depth maps paired with the low-quality depth maps and use the proposed evaluation framework, we use the camera poses corresponding to the images from the set L for rendering. To filter out bad pairs, caused by misalignments of camera poses w.r.t. the 3D model, we further split the depth maps into patches and followed a filtering strategy based on their structural similarity, as in [15]. Finally, we applied additional post-processing described in the supplementary material.

As described in Section 3.5, we split the patch pairs into train, validation and test sets, and Train A and Train B parts. We got 38,577 patch pairs in Train A, which we used to build the set L for unsupervised methods. However, since the filtering process described above retains only the low-quality patches with few missing values, we used 6,221 whole low-quality depth maps corresponding to the patches with more realistic low-quality data. We got 37,986 patch pairs in Train B, from which we built all three sets L, H, H_{down} for supervised methods, and the high-quality parts of which we used to build the sets H, H_{down} for unsupervised methods.

To build the **Testing dataset** we manually selected 501 whole images corresponding to patches with no misalignment and with the distribution of hole sizes similar to the

raw ScanNet. This was necessary for a more accurate evaluation of the ability of methods to fill in missing values.

For the second training dataset **ScanNet-InteriorNet** we built the low-quality source set L from the whole sensor images from ScanNet, and for the high-quality sets we used RGB-D images from InteriorNet [21].

Combining ScanNet-RenderScanNet and Testing dataset allows to compare paired and unpaired methods on the common data, while combining ScanNet-InteriorNet and Testing dataset allows to study the unpaired methods in a real-world unpaired learning scenario.

4.2. Experimental Results

In our experiments, we calculate pixel-wise metrics excluding the pixels without a definite ground truth value. To measure the denoising and inpainting performance specifically, we calculate RMSE_d , MAE_d and RMSE_h , MAE_h , taking into account only the pixels with definite low-quality depth values, and only the pixels without the value, *i.e.*, holes, respectively. RMSE and MAE are in millimeters.

Super-resolution. We consider the task of increasing a depth image resolution by a factor of two. We compare our method with a state-of-the-art supervised method for depth super-resolution MS-PFL [40] and a method for RGB image super-resolution SRFBN [23], applied to depth images. Originally, these methods are trained on pairs of high-quality images and their downsampled versions. We trained them in two scenarios: (1) on pairs from the sets L, H , *i.e.*, with low-quality sensor data as the input, and (2) on pairs from the sets H_{down}, H , *i.e.*, with the downsampled high-quality target as the input. Since the input in the Testing dataset consists of low-quality sensor data, the second scenario shows the performance in the wild of paired SR methods trained in a conventional way, on downsampled data.

To compare unsupervised methods with ours we combine them with upsampling. Since image-to-image unsupervised methods applied to depth maps produced relatively poor results for the enhancement task, *i.e.*, with the same image resolution of the input and output, as we discuss further, we report only the results produced by the enhancement method [8] combined with upsampling. We compare against several versions: (1) we train it on low-resolution depth maps from L, H_{down} , and for testing upsample its output with bicubic interpolation (denoted in tables as “[8] + B”), (2) or with SRFBN trained on pairs from L, H (denoted as “[8] + [23]”), or (3) train it on bicubically upsampled low-quality depth maps from L and high-resolution depth maps from H , and for testing apply it on top of bicubic interpolation (B + [8]).

The results on ScanNet-RenderScanNet in Table 3 and Figure 6b show that our method outperforms unsupervised methods and its performance is comparable to the supervised methods. The results on ScanNet-InteriorNet in Ta-

ble 5 and Figure 5b show that our unpaired approach could perform well on real sensor depth while being trained with synthetic data as examples of H data.

Enhancement. We compare the version of our method that does not change image resolution, with a state-of-the-art unsupervised method for depth enhancement from Gu *et al.* [8], as well as several RGB image translation methods: CycleGAN [49], U-GAT-IT [17] and NiceGAN [4]. We trained these methods on either 1-channel depth maps, or, in case of CycleGAN, also on 4-channel RGB-D images. We also compare our method with a state-of-the-art supervised method for depth enhancement LapDEN [15].

Table 2 and Figure 6a show the results for the ScanNet-RenderScanNet datasets. Our method successfully performs denoising and hole inpainting, and yields surface normals close to the target. It produces fewer artefacts in comparison to all unsupervised methods and preserves the original depth range in contrast to them. Quantitatively, our approach outperforms all unsupervised methods and is comparable to the supervised method.

We show some results on ScanNet-InteriorNet in Figure 5a and refer to the supplementary materials for the additional visualizations and quantitative comparisons.

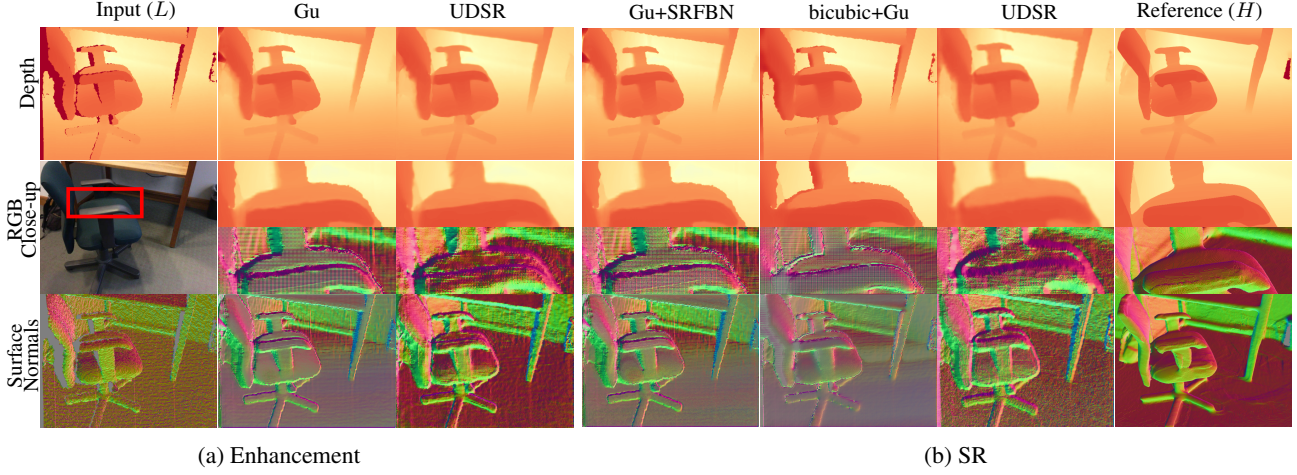
Ablation study.

In our ablation study, networks are trained on **ScanNet-InteriorNet**. We trained our approach with several modifications in *Translation Component* and *Enhancement Component*. The results are shown in Table 4. We demonstrate that to achieve low perceptual MSE_v we need use both generated pseudo-pairs and holes augmentation when training Enhancement Component u_{enh} . Further, with our *Translation Component* the method yields better results compared to using CycleGANs. An ablation study of the enhancement version of our method on **ScanNet-InteriorNet** can be found in the supplementary document.

5. Conclusions

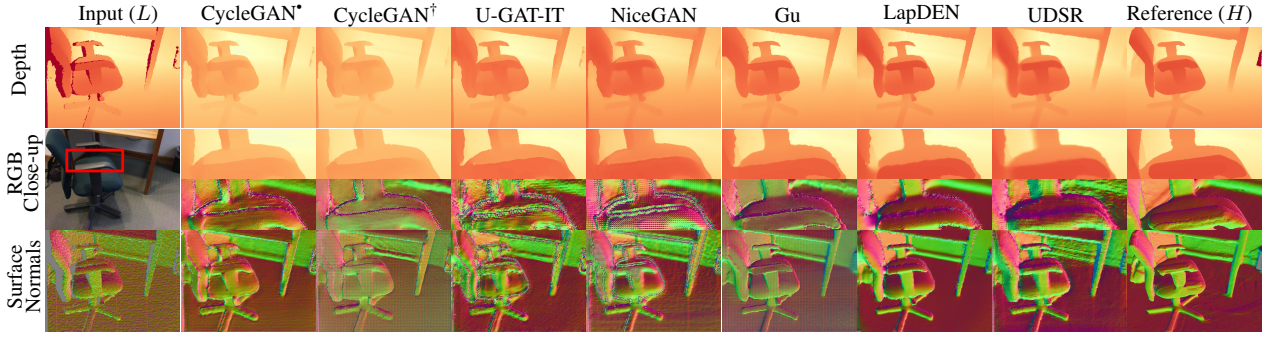
We have demonstrated how data-driven depth super-resolution and enhancement can be performed without using paired datasets, which, in turn, simplifies training models for this task on real-world depth map data. We constructed a benchmark for depth super-resolution based on real-world depth maps from ScanNet [5] and higher quality data obtained by rendering reconstructions obtained from multiple scans.

One important direction for future work is development of a paired test dataset with higher fidelity reference depth measurements, for more accurate validation and training. Although our method outperformed existing unpaired methods, we believe that performance can be further improved with fine-tuning the models. The improvement of the model robustness and scalability is another possible future direction.

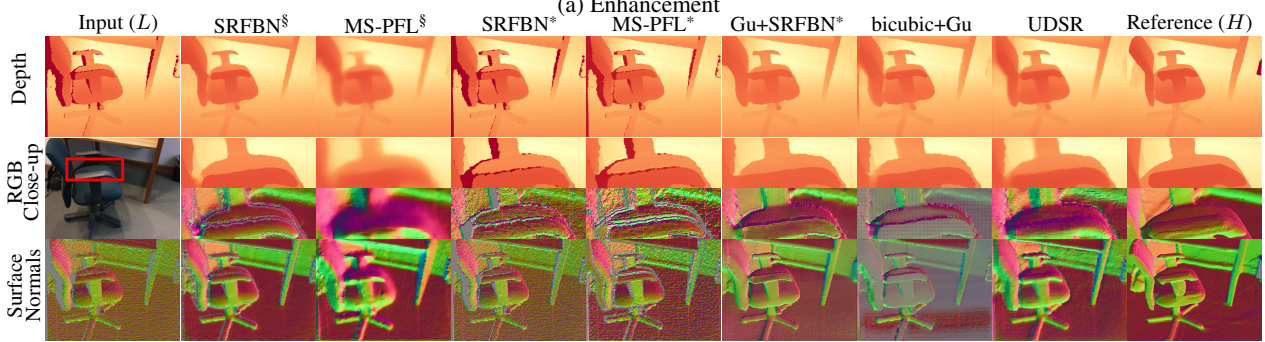


(a) Enhancement

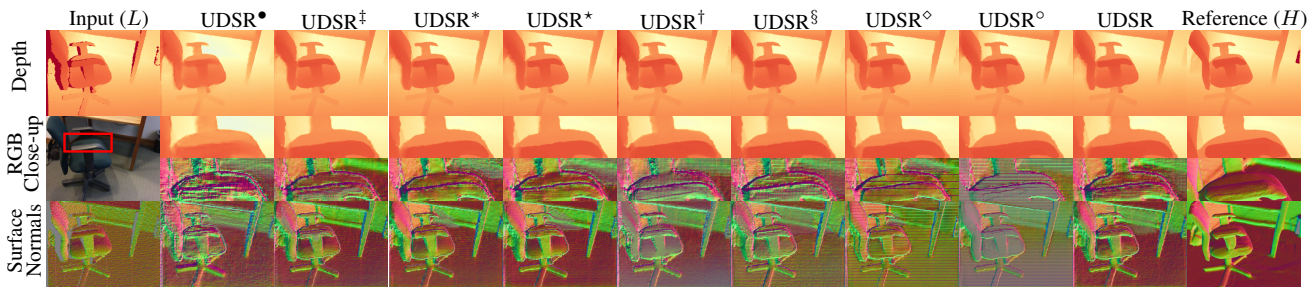
(b) SR

Figure 5: Enhancement and SR on **ScanNet-InteriorNet**.

(a) Enhancement



(b) SR

Figure 6: Enhancement and SR on **ScanNet-RenderScanNet**. [§] and ^{*} mark the models trained on (L, H) and (H_{down}, H) pairs respectively. ^{*} and [†] mark the models with the depth map input and depth map concatenated with RGB respectively.Figure 7: Ablation of SR on **ScanNet-InteriorNet**. Same notation as in Table 4.

References

- [1] Michal Irani, Assaf Shocher, Nadav Cohen. "zero-shot" super-resolution using deep internal learning. In *The IEEE Conference on Computer Vision and Pattern Recognition (CVPR)*, June 2018. 2
- [2] Adrian Bulat, Jing Yang, and Georgios Tzimiropoulos. To learn image super-resolution, use a gan to learn how to do image degradation first. In *Proceedings of the European Conference on Computer Vision (ECCV)*, September 2018. 1, 2, 3
- [3] Angel Chang, Angela Dai, Thomas Funkhouser, Maciej Halber, Matthias Niessner, Manolis Savva, Shuran Song, Andy Zeng, and Yinda Zhang. Matterport3d: Learning from rgbd data in indoor environments. *International Conference on 3D Vision (3DV)*, 2017. 3
- [4] Runfa Chen, Wenbing Huang, Binghui Huang, Fuchun Sun, and Bin Fang. Reusing discriminators for encoding: Towards unsupervised image-to-image translation. In *Proceedings of the IEEE/CVF Conference on Computer Vision and Pattern Recognition (CVPR)*, June 2020. 6, 7
- [5] Angela Dai, Angel X. Chang, Manolis Savva, Maciej Halber, Thomas Funkhouser, and Matthias Nießner. Scannet: Richly-annotated 3d reconstructions of indoor scenes. In *Proc. Computer Vision and Pattern Recognition (CVPR)*, IEEE, 2017. 2, 3, 6, 7
- [6] Angela Dai, Matthias Nießner, Michael Zollöfer, Shahram Izadi, and Christian Theobalt. Bundlefusion: Real-time globally consistent 3d reconstruction using on-the-fly surface re-integration. *ACM Transactions on Graphics 2017 (TOG)*, 2017. 2, 3, 6
- [7] David Ferstl, Christian Reinbacher, Rene Ranftl, Matthias Ruether, and Horst Bischof. Image guided depth upsampling using anisotropic total generalized variation. In *Proceedings of the IEEE International Conference on Computer Vision (ICCV)*, December 2013. 3
- [8] X. Gu, Y. Guo, F. Deligianni, and G. Yang. Coupled real-synthetic domain adaptation for real-world deep depth enhancement. *IEEE Transactions on Image Processing*, 29:6343–6356, 2020. 2, 3, 6, 7
- [9] Shi Guo, Zifei Yan, Kai Zhang, Wangmeng Zuo, and Lei Zhang. Toward convolutional blind denoising of real photographs. In *Proceedings of the IEEE/CVF Conference on Computer Vision and Pattern Recognition (CVPR)*, June 2019. 2
- [10] Bjoern Haefner, Songyou Peng, Alok Verma, Yvain Quéau, and Daniel Cremers. Photometric depth super-resolution. *IEEE Transactions on Pattern Analysis and Machine Intelligence*, 42(10):2453–2464, 2019. 2
- [11] Bjoern Haefner, Yvain Quéau, Thomas Möllenhoff, and Daniel Cremers. Fight ill-posedness with ill-posedness: Single-shot variational depth super-resolution from shading. In *Proceedings of the IEEE conference on computer vision and pattern recognition*, pages 164–174, 2018. 2
- [12] A. Handa, T. Whelan, J.B. McDonald, and A.J. Davison. A benchmark for RGB-D visual odometry, 3D reconstruction and SLAM. In *IEEE Intl. Conf. on Robotics and Automation, ICRA*, Hong Kong, China, May 2014. 3
- [13] Muhammad Haris, Greg Shakhnarovich, and Norimichi Ukita. Deep back-projection networks for super-resolution. In *IEEE Conference on Computer Vision and Pattern Recognition (CVPR)*, 2018. 1, 2
- [14] Tak-Wai Hui, Chen Change Loy, , and Xiaoou Tang. Depth map super-resolution by deep multi-scale guidance. In *Proceedings of European Conference on Computer Vision (ECCV)*, pages 353–369, 2016. 1, 2, 3
- [15] Junho Jeon and Seungyong Lee. Reconstruction-based pairwise depth dataset for depth image enhancement using cnn. In *Proceedings of the European Conference on Computer Vision (ECCV)*, September 2018. 1, 2, 3, 6, 7
- [16] Joohyeok Kim, Gwanggil Jeon, and Jechang Jeong. Joint-adaptive bilateral depth map upsampling. *Signal Processing: Image Communication*, 29(4):506–513, Apr. 2014. 2
- [17] Junho Kim, Minjae Kim, Hyeonwoo Kang, and Kwang Hee Lee. U-gat-it: Unsupervised generative attentional networks with adaptive layer-instance normalization for image-to-image translation. In *International Conference on Learning Representations*, 2020. 6, 7
- [18] Johannes Kopf, Michael F. Cohen, Dani Lischinski, and Matt Uyttendaele. Joint bilateral upsampling. *ACM Transactions on Graphics (Proceedings of SIGGRAPH 2007)*, 26(3), 2007. 2
- [19] Stamatios Lefkimiatis. Non-local color image denoising with convolutional neural networks. In *Proceedings of the IEEE Conference on Computer Vision and Pattern Recognition (CVPR)*, July 2017. 2
- [20] Stamatios Lefkimiatis. Universal denoising networks : A novel cnn architecture for image denoising. In *Proceedings of the IEEE Conference on Computer Vision and Pattern Recognition (CVPR)*, June 2018. 2
- [21] Wenbin Li, Sajad Saeedi, John McCormac, Ronald Clark, Dimos TZoumanikas, Qing Ye, Yuzhong Huang, Rui Tang, and Stefan Leutenegger. Interiornet: Mega-scale multi-sensor photo-realistic indoor scenes dataset. In *British Machine Vision Conference (BMVC)*, 2018. 2, 3, 7
- [22] Yijun Li, Jia-Bin Huang, Ahuja Narendra, and Ming-Hsuan Yang. Deep joint image filtering. In *European Conference on Computer Vision*, 2016. 2
- [23] Zhen Li, Jinglei Yang, Zheng Liu, Xiaomin Yang, Gwanggil Jeon, and Wei Wu. Feedback network for image super-resolution. In *Proceedings of the IEEE/CVF Conference on Computer Vision and Pattern Recognition (CVPR)*, June 2019. 1, 2, 6, 7
- [24] Guilin Liu, Fitzsum A. Reda, Kevin J. Shih, Ting-Chun Wang, Andrew Tao, and Bryan Catanzaro. Image inpainting for irregular holes using partial convolutions. In *The European Conference on Computer Vision (ECCV)*, 2018. 2
- [25] Cheng Ma, Yongming Rao, Yean Cheng, Ce Chen, Jiwen Lu, and Jie Zhou. Structure-preserving super resolution with gradient guidance. In *Proceedings of the IEEE/CVF Conference on Computer Vision and Pattern Recognition (CVPR)*, June 2020. 1, 2
- [26] Shunta Maeda. Unpaired image super-resolution using pseudo-supervision. In *Proceedings of the IEEE/CVF Conference on Computer Vision and Pattern Recognition (CVPR)*, June 2020. 1, 2, 3, 4

[27] Xudong Mao, Qing Li, Haoran Xie, Raymond Y.K. Lau, Zhen Wang, and Stephen Paul Smolley. Least Squares Generative Adversarial Networks. In *2017 IEEE International Conference on Computer Vision (ICCV)*, pages 2813–2821, Venice, Oct. 2017. IEEE. 4

[28] Pushmeet Kohli, Nathan Silberman, Derek Hoiem and Rob Fergus. Indoor segmentation and support inference from rgbd images. In *ECCV*, 2012. 3

[29] Jaesik Park, Qian-Yi Zhou, and Vladlen Koltun. Colored point cloud registration revisited. In *ICCV*, 2017. 3

[30] Yurui Ren, Xiaoming Yu, Ruonan Zhang, Thomas H. Li, Shan Liu, and Ge Li. Structureflow: Image inpainting via structure-aware appearance flow. In *IEEE International Conference on Computer Vision (ICCV)*, 2019. 2

[31] Gernot Riegler, David Ferstl, Matthias Rüther, and Bischof Horst. A deep primal-dual network for guided depth super-resolution. In *British Machine Vision Conference*, 2016. 5

[32] Gernot Riegler, Matthias Rüther, and Bischof Horst. Atgv-net: Accurate depth super-resolution. In *European Conference on Computer Vision*, 2016. 1, 2

[33] Olaf Ronneberger, Philipp Fischer, and Thomas Brox. U-net: Convolutional networks for biomedical image segmentation. In Nassir Navab, Joachim Hornegger, William M. Wells III, and Alejandro F. Frangi, editors, *Medical Image Computing and Computer-Assisted Intervention - MICCAI 2015 - 18th International Conference Munich, Germany, October 5 - 9, 2015, Proceedings, Part III*, volume 9351 of *Lecture Notes in Computer Science*, pages 234–241. Springer, 2015. 5

[34] Daniel Scharstein, Heiko Hirschmüller, York Kitajima, Greg Krathwohl, Nera Nešić, Xi Wang, and Porter Westling. High-resolution stereo datasets with subpixel-accurate ground truth. In *German Conference on Pattern Recognition*, pages 31–42. Springer, 2014. 3

[35] Akhmedkhan Shabanov, Ilya Krotov, Nikolay Chinaev, Vsevolod Poletaev, Sergei Kozlukov, Igor Pasechnik, Bulat Yakupov, Artsiom Sanakoyeu, Vadim Lebedev, and Dmitry Ulyanov. Self-supervised depth denoising using lower- and higher-quality RGB-D sensors. In *8th International Conference on 3D Vision (3DV)*, pages 743–752. IEEE, 2020. 3

[36] Shuran Song, Samuel P. Lichtenberg, and Jianxiong Xiao. Sun rgb-d: A rgb-d scene understanding benchmark suite. In *Proceedings of the IEEE Conference on Computer Vision and Pattern Recognition (CVPR)*, June 2015. 3

[37] Xibin Song, Yuchao Dai, Dingfu Zhou, Liu Liu, Wei Li, Hongdong Li, and Ruigang Yang. Channel attention based iterative residual learning for depth map super-resolution. In *Proceedings of the IEEE/CVF Conference on Computer Vision and Pattern Recognition (CVPR)*, June 2020. 1, 2

[38] Vladimiros Sterzentsenko, Leonidas Saroglou, Anargyros Chatzitofis, Spiros Thermos, Nikolaos Zioulis, Alexandros Doumanoglou, Dimitrios Zarpalas, and Petros Daras. Self-Supervised Deep Depth Denoising. In *2019 IEEE/CVF International Conference on Computer Vision (ICCV)*, pages 1242–1251, Seoul, Korea (South), Oct. 2019. IEEE. 1, 3

[39] Oleg Voynov, Alexey Artemov, Vage Egiazarian, Alexander Notchenko, Gleb Bobrovskikh, Evgeny Burnaev, and Denis Zorin. Perceptual deep depth super-resolution. In *Proceedings of the IEEE International Conference on Computer Vision (ICCV)*, pages 5653–5663, 2019. 1, 2, 3, 4, 5

[40] Chuhua Xian, Kun Qian, Zitian Zhang, and Charlie C. L. Wang. Multi-Scale Progressive Fusion Learning for Depth Map Super-Resolution. *arXiv e-prints*, page arXiv:2011.11865, Nov. 2020. 1, 2, 6, 7

[41] Fuzhi Yang, Huan Yang, Jianlong Fu, Hongtao Lu, and Baineng Guo. Learning texture transformer network for image super-resolution. In *Proceedings of the IEEE/CVF Conference on Computer Vision and Pattern Recognition (CVPR)*, June 2020. 1, 2

[42] W. Yang, X. Zhang, Y. Tian, W. Wang, J. Xue, and Q. Liao. Deep learning for single image super-resolution: A brief review. *IEEE Transactions on Multimedia*, 21(12):3106–3121, 2019. 1, 2

[43] Zili Yi, Qiang Tang, Shekoufeh Azizi, Daesik Jang, and Zhan Xu. Contextual residual aggregation for ultra high-resolution image inpainting. In *Proceedings of the IEEE/CVF Conference on Computer Vision and Pattern Recognition (CVPR)*, June 2020. 2

[44] Jiahui Yu, Zhe Lin, Jimei Yang, Xiaohui Shen, Xin Lu, and Thomas S. Huang. Generative image inpainting with contextual attention. In *Proceedings of the IEEE Conference on Computer Vision and Pattern Recognition (CVPR)*, June 2018. 2

[45] Yuan Yuan, Siyuan Liu, Jiawei Zhang, Yongbing Zhang, Chao Dong, and Liang Lin. Unsupervised image super-resolution using cycle-in-cycle generative adversarial networks. In *Proceedings of the IEEE Conference on Computer Vision and Pattern Recognition (CVPR) Workshops*, June 2018. 1, 2, 5

[46] Kai Zhang, Wangmeng Zuo, Yunjin Chen, Deyu Meng, and Lei Zhang. Beyond a Gaussian denoiser: Residual learning of deep CNN for image denoising. *IEEE Transactions on Image Processing*, 26(7):3142–3155, 2017. 2

[47] Yinda Zhang and Thomas Funkhouser. Deep Depth Completion of a Single RGB-D Image. In *2018 IEEE/CVF Conference on Computer Vision and Pattern Recognition*, pages 175–185, Salt Lake City, UT, USA, June 2018. IEEE. 2

[48] Chuanxia Zheng, Tat-Jen Cham, and Jianfei Cai. T2net: Synthetic-to-realistic translation for solving single-image depth estimation tasks. In *Proceedings of the European Conference on Computer Vision (ECCV)*, pages 767–783, 2018. 5

[49] Jun-Yan Zhu, Taesung Park, Phillip Isola, and Alexei A. Efros. Unpaired image-to-image translation using cycle-consistent adversarial networks. In *Proceedings of the IEEE International Conference on Computer Vision (ICCV)*, Oct 2017. 2, 6, 7